Annals of Biomedical Engineering, Vol. 27, pp. 391–402, 1999
Printed in the USA.

0090-6964/99/27(3)/391/12/$15.00

Principal Dynamic Mode Analysis of Nonlinear Transduction in a Spider Mechanoreceptor

VASILIS Z. MARMARELIS,[1] MIKKO JUUSOLA,[2] and ANDREW S. FRENCH[2]

[1]Department of Biomedical Engineering, USC, Los Angeles, CA and [2]Department of Physiology and Biophysics, Dalhousie University, Halifax, Canada

(Received 6 January 1998; accepted 22 January 1999)

Abstract—The nonlinear dynamics of the mechanoelectrical transduction in an arthropod mechanoreceptor (cuticular slit sense organ of the spider *Cupiennius salei*) were studied using Volterra kernel measurements and the recently proposed method of principal dynamic modes. Since mechanoreceptors must operate with sufficient gain sensitivity to rapidly varying displacement stimuli over a broad bandwidth and for a wide range of amplitudes, the experimental data were generated by applying pseudorandom broadband mechanical displacements of various mean levels to the cuticular slits. The recorded response data were intracellular current and potential. The purpose of this paper is to demonstrate the use of the principal dynamic mode (PDM) methodology in elucidating the nonlinear dynamics of a spider mechanoreceptor. The results obtained demonstrate that two PDMs suffice to provide a complete nonlinear dynamic model of this insect mechanoreceptor. The first PDM resembles the first-order kernel and has a low pass characteristic (position dependent), while the second PDM has a high-pass characteristic (velocity-dependent) and resides entirely in the second-order kernel (nonlinear adaptation). This study may serve as an example of the proper use of this new methodology for the analysis of nonlinear physiological systems. © *1999 Biomedical Engineering Society.*
[S0090-6964(99)01703-8]

Keywords—Nonlinear modeling, Volterra kernels, Laguerre expansion, Nonlinear adaptation.

INTRODUCTION

The transduction and detection of mechanical stimuli occurs in many animal tissues and is used widely for both sensory and regulatory purposes. As in other sensory modalities, mechanoreceptors must operate with sufficient gain to detect small stimuli, but at the same time provide an operating range that can accommodate most naturally occurring stimuli, leading to systems that can adapt their gains to the prevailing stimulus conditions. In addition, a variety of dynamic behavior is seen, which presumably reflects the varying functional roles of mechanoreceptors. The overall dynamic behaviors of mechanoreceptors, and the molecular mechanisms involved, are not yet well understood, mainly because of the small physical size and inaccessibility of most mechanoreceptors.

In previous work we used the principal dynamic mode (PDM) methodology to characterize the nonlinear dynamic behavior of action potential encoding in an insect mechanoreceptor.[2] We have now used the PDM approach to examine the most fundamental stage of mechanoreception; the conversion of mechanical displacement into transmembrane receptor current, in an arthropod mechanoreceptor. Single neurons of a slit-sense organ in the spider, *Cupiennius salei*, were stimulated with pseudorandom broadband displacements of varying mean levels to simulate the range of natural stimulation, while intracellular microelectrodes were used to observe the resulting receptor current under voltage clamp or the receptor potential under current clamp.

This work demonstrates the use of the PDM technique to characterize the nonlinear dynamic behavior of a biological system and should serve as an example of the proper use of this new methodology for the general study of nonlinear physiological systems, and a guide to the interpretation of the resulting characterization.

METHODS

Experimental Preparation

A calibrated mechanical stimulus was applied to a defined position on a slit of the cuticular slit sense organ mechanoreceptors. Motion of the stimulating probe compressed the cuticular slits, causing their local displacement relative to the surrounding cuticle, thus subjecting the sensory endings of the bipolar mechanoreceptor neurons to mechanical displacement. A leg from adult female tropical hunting spiders (*C. salei*) was autotomized and a concave piece of cuticule containing lyrifom organ VS-3 was dissected from the anterior patella and prepared under a microscope. Full details of this preparation

Address correspondence to Professor Vasilis Marmarelis, Department of Biomedical Engineering, University of Southern California, University Park–OHE 500, Los Angeles, CA 90089-1451. Electronic mail: vzm@bmsrs.usc.edu

are given in Ref. 12. The slit sense organ preparation was fixed with beeswax onto a custom-designed Plexiglas holder. The interior concave surface of a fixed preparation was connected to the holder's bath chamber, filled with fresh spider saline (pH 8.2), and grounded with an indifferent electrode (silver–silver chloride). An additional manipulator was used for lowering small tubes into the holder's bath so that fresh saline, with or without 10 μM tetrodotoxin (TTX), could be added when needed. The preparation-holder complex was firmly held by a stand while the mechanical stimulus was applied to the exterior surface of the preparation from below. The stimulator was a modified loudspeaker with servocontrolled position and an infrared optical position indicator circuit. Computer-generated voltage commands (pseudorandom modulation) drove the stimulator. The resulting displacement was applied to the slit sense organ by a small insect pin grounded so as to reduce electrical noise from the stimulator. The pin tip was seen under illumination through the transparent cuticle and its location could be altered by a three-dimensional micromanipulator.

The stimuli were measured by the displacement (micrometers) of the pin tip, read from the output of the optical position indicator, and recorded with a microcomputer (IBM 386 compatible) using an ASYST (Keithley)-based program.[4] The actual stimulus delivered by the stimulator was band limited and pseudorandomly modulated with a Gaussian amplitude distribution and spectrally flat up to $\sim$400 Hz. Current- or voltage-clamp recordings were obtained from mechanoreceptor somata using single microelectrodes filled with 3 M KCl and having resistances between 25 and 80 MΩ when in the tissue. The microelectrodes were connected to a single-electrode voltage-clamp amplifier (SEC-10L, NPI Electronics, Germany). The frequency response of the recording system, including the microelectrode, had a 3-dB high-frequency cutoff at $\geqslant$10 kHz.[4]

The sensitivity of the neurons was tested by 200- to 300-ms step displacements of the slits. The stimuli were directed to the slit that gave the maximum receptor potential (or generator potential) with superimposed action potentials. This was usually the slit that was seen to be innervated by the neuron. If the voltage responses were adequate (resting potential less than -60 mV, action potential amplitudes >50 mV), 10 μM TTX was added to the bath to suppress the fast voltage-activated sodium current. A period of 2–5 min was normally required for all action potentials to be suppressed. TTX has no effect on the receptor current.[3] The adaptation properties of the neurons were then studied under voltage clamp by observing the dynamics of the receptor current during displacement stimuli. In these experiments, the neurons were allowed to adapt for 10 s to a preselected constant displacement background applied to the slit before superimposing the pseudorandomly modulated displacement. This adaptation period was sufficient to complete the adaptational decay of the receptor current and so to ensure that the sensitivity of the mechanoreceptors had reached a steady level. The recovery from adaptation and the responses to displacement steps and pseudorandom modulation were repeatable within a displacement range of <20 μm from one preparation to another. In general, the preparations were stable for a period of $\geqslant$1 h and occasionally several recordings were obtained from the same neuron.

The sampling at 1 kHz of the electrical responses was initiated synchronously to the onset of the pseudorandom signal produced by the computer. Records of the cell response and the stimulating pin position obtained during each cycle were digitized with a 12-bit A–D converter (DT2821, Data Translation), converted to suitable units (mV or nA for responses; μm for displacements), and stored on a disk. A 6 s interval of mean steady background displacement was maintained between each consecutive run to ensure that adaptation was equal for each stimulus sequence. Pseudorandom displacement stimuli from a shift-register generator were applied for periods of 8.192 s. Responses were averaged 10 times.

Analysis Methodology

Four data sets of 4000 datapoints sampled at 1 kHz (4 s long) of the mechanical random forcing input and the intracellular current or potential output were used to estimate the first- and second-order Volterra kernels via the Laguerre expansion technique.[8] The kernels were estimated over 50 ms (memory) and validated by model prediction of four test data sets (not used for estimation) for each case of output data (current or potential). These kernel estimates were used, in turn, to compute the PDMs of the system.[9] Having computed the PDMs, we estimated the associated nonlinearity for each system.[9] An outline of the methodology is provided in Appendix A for the convenience of the reader. All computations were performed on a Pentium-based PC system running the LYSIS software package under Microsoft Windows, which has been developed by the Biomedical Simulations Resource at the University of Southern California under NIH sponsorship.

RESULTS

Using four data sets of intracellular recordings of induced current, we first estimate the first- and second-order kernels via the Laguerre expansion technique.[8] The resulting first-order kernel estimates for two representative recordings are shown in Fig. 1 in the time and frequency domains, exhibiting consistent waveforms but different amplitudes, due to the fact that the two record-

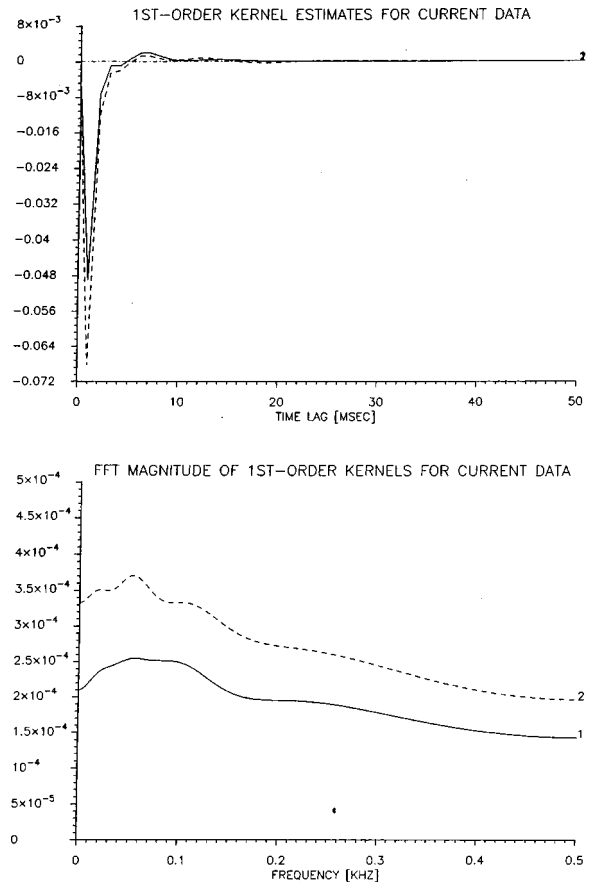

FIGURE 1. The obtained first-order kernel estimates using intracellular current response data (under voltage-clamped conditions) in the time (top) and frequency (bottom) domains, for two different mean displacement stimulus levels (solid: 29.02; dashed: 31.90). The peak kernel value for the higher mean displacement level is about 40% larger; but the waveforms of the two kernels are similar, exhibiting mildly low-pass characteristics. The ordinate axis units for the first-order kernel are: nA/(μm ms).

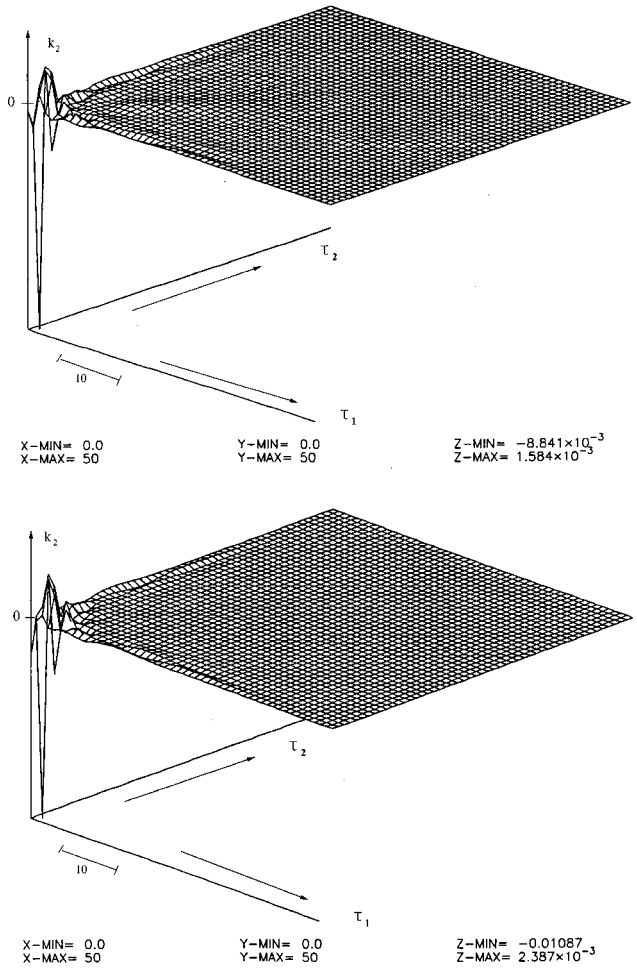

FIGURE 2. The obtained second-order kernel estimates in the time domain for the two data sets discussed in Fig. 1. The peak-to-peak kernel value for the higher mean displacement level is about 25% larger; but the waveforms of the two kernels are similar. The ordinate axis units for the second-order kernel are: nA/(μm ms)^2. The τ_1 and τ_2 axes are in millisecond units (10 ms bar shown).

ings have different mean displacement values (i.e., average stimulus levels) that define different operating points with distinct gain sensitivities.[5] Specifically, the kernel corresponding to the higher mean displacement level is about 40% larger (solid: 29.02; dashed: 31.90) and has slightly smaller stimulus power (solid: 0.798; dashed: 0.764). The frequency response of the kernels peaks at about 50 Hz and declines gradually above 100 Hz. What is most intriguing in Fig. 1 is that the frequency response characteristics of both first-order kernels are mildly low pass, although the apparent transfer function magnitude for this preparation has been reported previously to exhibit marked high-pass characteristics above 150 Hz.[5] This apparent inconsistency can be explained by the high-pass frequency response characteristics of the second-order Volterra model term governed by the second-order kernel, as illustrated below. Note that the high-pass characteristics of the nonlinear terms are reflected on the apparent transfer function measurement,[7] thus the latter does not represent the linear dynamics of the system. This is a good example of the pitfalls of linearized analysis.

The obtained second-order kernel estimates for the same two recordings are shown in the time domain in Fig. 2, also exhibiting similar forms but different amplitudes that follow a similar size relation with their first-order counterparts (i.e., about 25% larger for the higher mean displacement level). The contribution of the second-order kernel to the system response is significant relative to the first-order kernel contribution for this system, as illustrated for a segment of high mean displacement data in Fig. 3, where the actual system response (trace 1) is compared to the model predictions of first- (trace 2) and second order (trace 3). The normalized

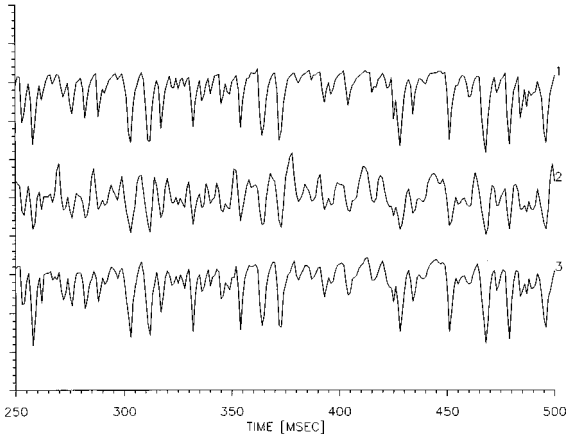

FIGURE 3. Model predictions for a segment of high mean displacement data not used for kernel estimation. Actual current response data (trace 1), first-order model prediction (trace 2) and second-order model prediction (trace 3). The significant contribution of the second-order kernel to the current response is visually evident. The normalized mean-square errors are: 34.1% for the first-order, and 8.3% for the second-order model prediction. The ordinate axis units are: nA.

mean-square errors (NMSE) are: 34.1% for the first order and 8.3% for the second-order model (the latter includes the first- and second-order kernels). Note that this comparison is made with a segment of data not used for the estimation of the kernels for each experiment. The comparison demonstrates the inadequacy of the first-order (linear) model and the good prediction obtained by the second-order model.

Next we compute the PDMs (modes) of this system using the first- and second-order kernel estimates.[9] Only two significant modes are found in this system and they are shown in Fig. 4 for the aforementioned two recordings. The consistency in the form of these modes for different recordings is remarkable. The corresponding eigenvalues for the first (λ_1) and second (λ_2) modes are ($\lambda_1=-0.0317$, $\lambda_2=-0.0046$) and ($\lambda_1=-0.0632$, $\lambda_2=0.0078$) for the two recordings, indicating the relative contributions of the two modes to the system output (the first is about one order of magnitude larger). The two modes are shown in the frequency domain (FFT magnitude) in Fig. 5 and demonstrate the high-pass characteristics of the second mode (evident in the second-order kernel), and the mildly low-pass characteristics of the first mode that resembles the first-order kernel. This result also demonstrates that the high-pass characteristics of the mechanoreceptor reside in the second-order kernel and not in the first-order kernel, i.e., the high-pass behavior is strictly nonlinear! Therefore, the fundamental property of adaptation characterizing the mechanoreceptor response (i.e., the fact that the system retains gain sensitivity when the mean displacement changes) is strictly nonlinear.

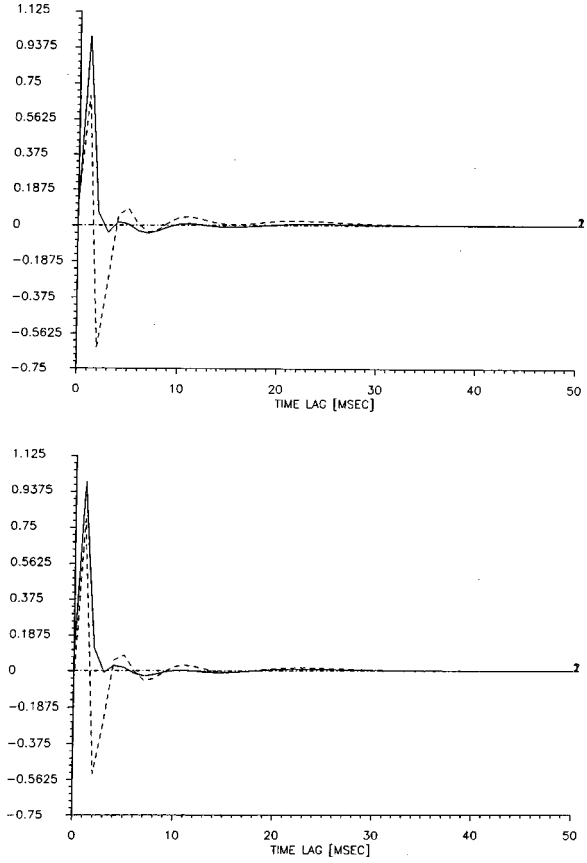

FIGURE 4. The computed two principal dynamic modes (PDM) in the time domain using the intracellular current kernels of Figs. 1 and 2. The PDMs for the two mean displacement levels (low: top; high: bottom) are rather similar. The waveform of the first PDM (solid) is similar to the first-order kernel (with reverse polarity) exhibiting mild low-pass characteristics, while the second PDM (dashed) exhibits strong high-pass characteristics, as illustrated in Fig. 5. The corresponding eigenvalues are both negative and indicate that the contribution of the first PDM to the current response is about one order of magnitude larger than the contribution of the second PDM. The ordinate axis units for the PDMs are: nA/(μm ms).

The nonlinearity associated with these two modes is shown in Fig. 6 in 3D perspective. It is evident from this plot that the nonlinear dependence of the system output (intracellular current) upon the first mode output, u_1, follows a ramp-threshold characteristic whose critical point (threshold value) remains fairly constant and close to zero for positive values of the second mode output, u_2, but rapidly decreases for negative values of u_2. This nonlinear surface is concave (negative eigenvalues) reflecting the fact that the differential change of intracellular current in response to an increase of displacement forcing is negative. Note also that the slope of the ramp–threshold curve with respect to u_1 decreases with decreasing u_2. The form of this nonlinearity indicates directionally selective behavior of the mechanoreceptor, since the response characteristics with respect to u_1

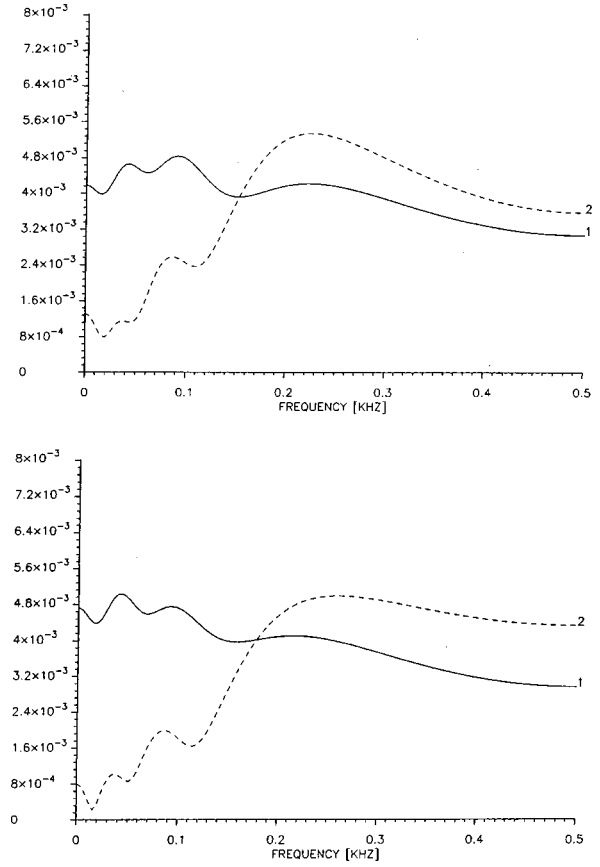

FIGURE 5. The two computed PDMs for the intracellular current data in the frequency domain (i.e., FFT magnitude of the PDMs shown in Fig. 4). The high-pass characteristic of the second PDM is not evident in the first-order kernel (i.e., it resides entirely in the second-order kernel), indicating nonlinear adaptation of the mechanoreceptor.

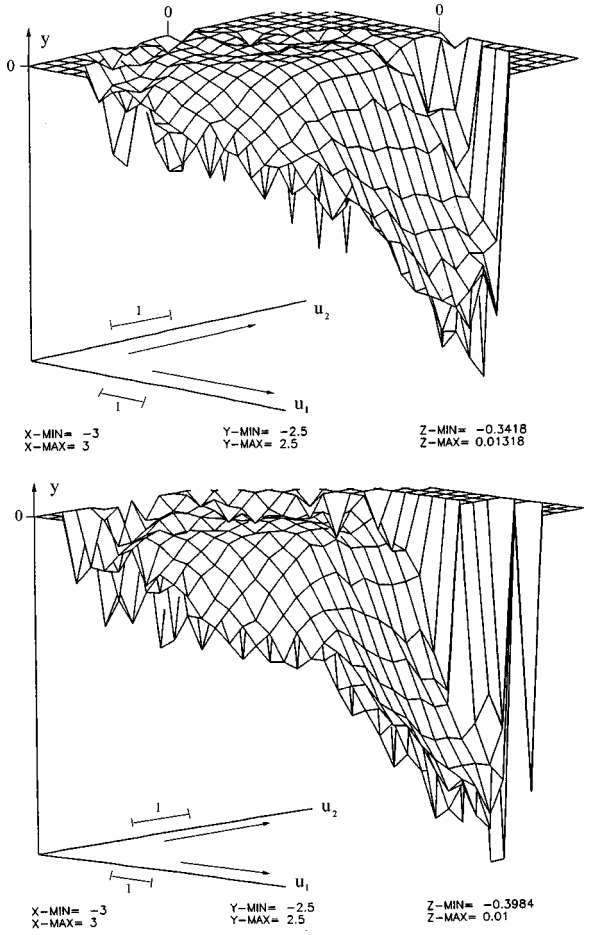

FIGURE 6. The static nonlinearities associated with the two PDMs of Figs. 4 and 5: high mean level (bottom), low mean displacement level (top). The axes (u_1, u_2) represent the two PDM outputs. The vertical axis is the intracellular current response (negative). The axes ranges are given at the bottom of each plot. The ramp-threshold concave characteristic with respect to u_1 is evident, as well as the asymmetry with respect to u_2. The ordinate axis units are: nA. The u_1 and u_2 axes are also in nA units (1 nA bar shown).

(magnitude of displacement) are distinctly different for negative and positive values of u_2 (change of displacement).

This interesting nonlinearity and the associated two modes constitute a complete nonlinear model for the system defined by the mechanical displacement input and the intracellular current output (under voltage-clamped conditions).

We now turn to the intracellular potential data collected under current-clamped conditions. Here too the results have been very consistent in form across recordings. Two representative first-order kernels, obtained for the same stimuli used in the two previously presented current recordings are shown in Fig. 7 in the time and frequency domains. These first-order kernels look like low-pass filtered versions of their intracellular current counterparts of Fig. 1 (due to the transmembrane capacitance) but their size relation is more exaggerated in favor of the higher mean displacement level case (i.e., the peak value of the corresponding kernel is about double—compared to about 40% larger for the current output case). The corresponding second-order kernels are shown in the time domain in Fig. 8. The consistency in the form of these kernels is again evident, and the size relation is similar to their first-order kernel counterparts of Fig. 7. The first- and second-order model predictions are shown in Fig. 9 along with the actual output for a segment of data not used for the estimation of the kernels. The significant contribution of the second-order kernel is again evident (NMSE for second-order prediction is 25.9% versus 60.2% for the first-order prediction), demonstrating the inadequacy of the linear (first-order) model.

Computation of the modes from these kernel estimates again yields only two significant modes for this system, shown in Fig. 10 for the same two recordings. We observe that the first modes are now more strongly

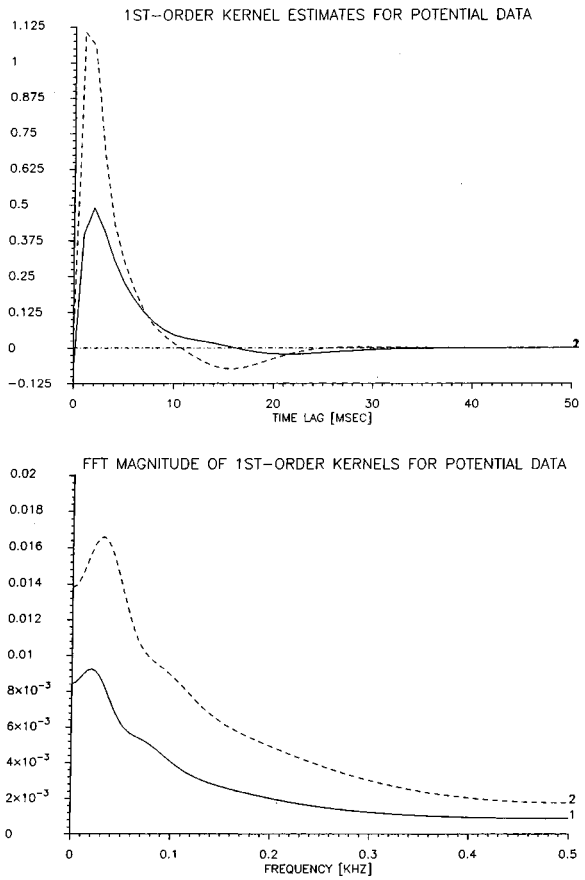

FIGURE 7. The obtained first-order kernel estimates using intracellular potential response data (under current-clamped conditions) in the time (top) and frequency (bottom) domains, for the same stimuli as in Fig. 1. These first-order kernels look like low-pass versions of their intracellular current counterparts in Fig. 1 (due to the transmembrane capacitance), although the size relation is more exaggerated in favor of the higher mean displacement level case. The ordinate axis units for the first-order kernel are: mV/(μm ms).

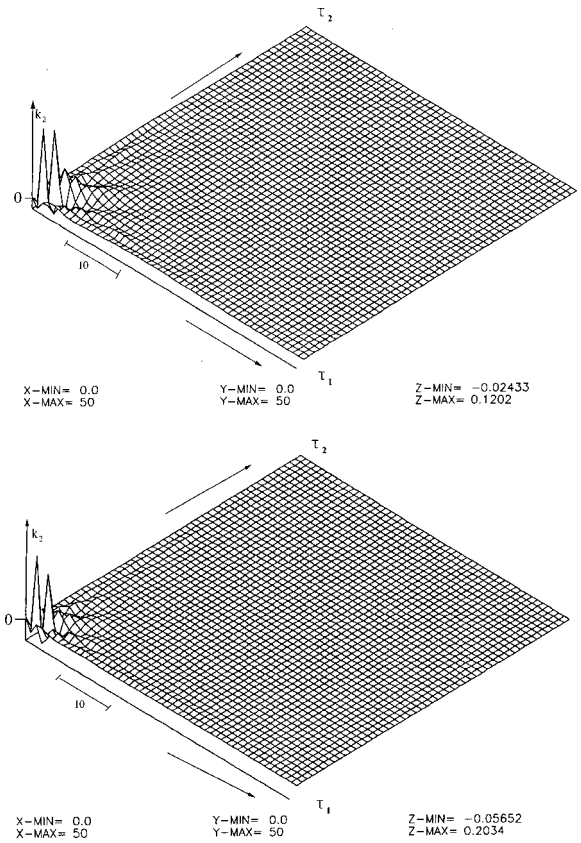

FIGURE 8. The obtained second-order kernel estimates in the time domain for the two data sets discussed in Fig. 7. The waveforms are similar for the two mean displacement levels, but the size for the higher mean displacement level is about double—in rough correspondence to their first-order kernel counterparts. The ordinate axis units for the second-order kernel are: mV/(μm ms)^2. The τ_1 and τ_2 axes are in ms units (10 ms bar shown).

low pass, resembling the first-order kernel waveforms, while the second modes remain distinctly high pass, and notably similar in waveform (although of reverse polarity) to the second modes of the previously analyzed current data. The corresponding eigenvalues for the first (λ_1) and second (λ_2) modes are (λ_1=2.877, λ_2=0.145) and (λ_1=2.649, λ_2=0.247) for the two recordings, indicating the relative contributions of the two modes to the system output (the first is about one order of magnitude larger). These modes are shown in the frequency domain (FFT magnitude) in Fig. 11. Clearly the first mode dominates up to about 150 Hz and the second mode is dominant above that frequency. Thus, for the intracellular potential data, the two modes seem to divide the operational bandwidth at about 150 Hz.

The nonlinearities associated with the two modes for the intracellular potential data at the aforementioned two different mean displacement levels are shown in Fig. 12 in 3D perspective. It is evident from these plots that the nonlinear surface is convex, reflecting the fact that the differential change of intracellular potential in response to an increase of displacement forcing is positive (this is also the reason for the positive eigenvalues). The form of the nonlinear surface changes slightly with mean displacement level (in addition to the obvious and anticipated change in elevation). This nonlinearity and the associated two modes constitute a complete nonlinear dynamic model of the system defined by the mechanical forcing (displacement) input and the intracellular potential output under current-clamped conditions.

CONCLUSIONS

These results demonstrate the efficacy and the utility of principal dynamic mode analysis (based on second-order Volterra models) in enhancing our understanding of the nonlinear dynamic behavior of the mechanoreceptor system. The key results are as follows.

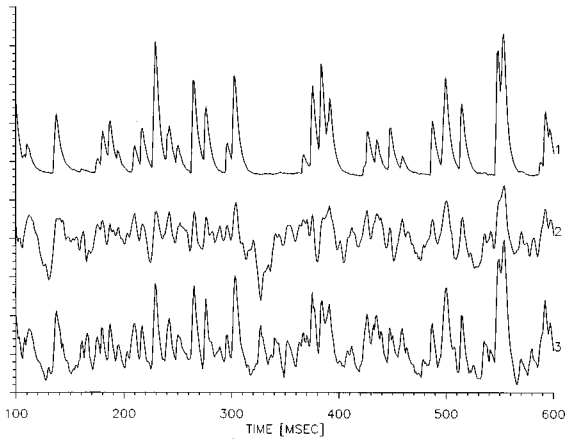

FIGURE 9. A segment of intracellular potential test data (trace 1) and the model predictions of first-order (trace 2) and second-order (trace 3). The significant contribution of the second-order kernel to the response potential is evident. The normalized mean-square errors are: 60.2% for the first-order, and 25.9% for the second-order model prediction. The ordinate axis units are: mV.

(1) Consistent kernel estimates of first and second order across recordings.

(2) Inadequacy of the first-order (linear) model and significant contribution of the second-order kernel, based on respective predictions of the system response.

(3) Significant increase in the size of the kernel estimates (and of the system response) when the mean level of the displacement stimulus increases, although the respective stimulus power decreases slightly (i.e., higher gain sensitivity).

(4) Consistent estimates of two significant principal dynamic modes: one with low pass and the other with high-pass frequency response characteristics, for both intracellular current and potential response data (under voltage- and current-clamped conditions, respectively).

(5) The first mode (low pass) is similar in waveform to the first-order kernel; and the second mode resides entirely in the second-order kernel (the latter also contains the first mode). Thus, the high-pass characteristics of the mechanoreceptor (represented by the second mode and responsible for its adaptation property) are entirely a nonlinear mechanism.

(6) The first mode for the intracellular potential data is a low-pass filtered version of its counterpart for the current data (as expected, due to the membrane capacitance).

(7) The second modes (high pass) for current and potential data are notably similar in waveform (although of reverse polarity), dominating the response characteristics of the mechanoreceptor above approximately 150 Hz.

(8) For the intracellular potential data, the two modes appear to divide the frequency response bandwidth at about 150 Hz (first mode is dominant below 150 Hz; second mode is dominant above 150 Hz).

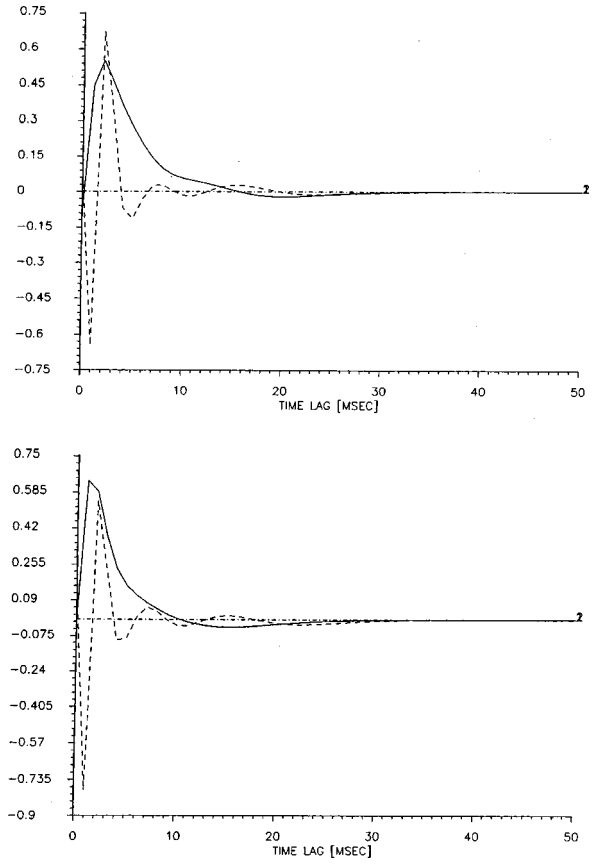

FIGURE 10. The two computed PDMs in the time domain, using the intracellular potential kernels of Figs. 7 and 8. Again the waveforms are similar for the two mean displacement levels, and the first PDMs (solid) resemble in waveform the first-order kernels. The second PDMs (dashed) are similar in waveform to their counterparts for the intracellular current data (with reverse polarity). The corresponding eigenvalues are both positive and indicate that the relative contribution of the first PDM is about one order of magnitude larger. The ordinate axis units for the PDMs are: mV/(μm ms).

(9) The nonlinearities associated with the two modes are distinct for current and potential data and exhibit concave and convex morphologies, respectively. The form of these nonlinearities changes only slightly for various mean displacement stimulus levels (with the curvature somewhat blunted for higher mean displacement stimulus levels), except for a significant (and anticipated) change in elevation.

(10) A plateau of low values (deviations from the mean response level) is evident for negative values of the first mode output and nonlinear dependence is evident for positive values, implying a threshold characteristic in the position dependence of the mechanoreceptor response. The velocity dependence (represented by the second mode output) is measurable and nonlinear but not as pronounced.

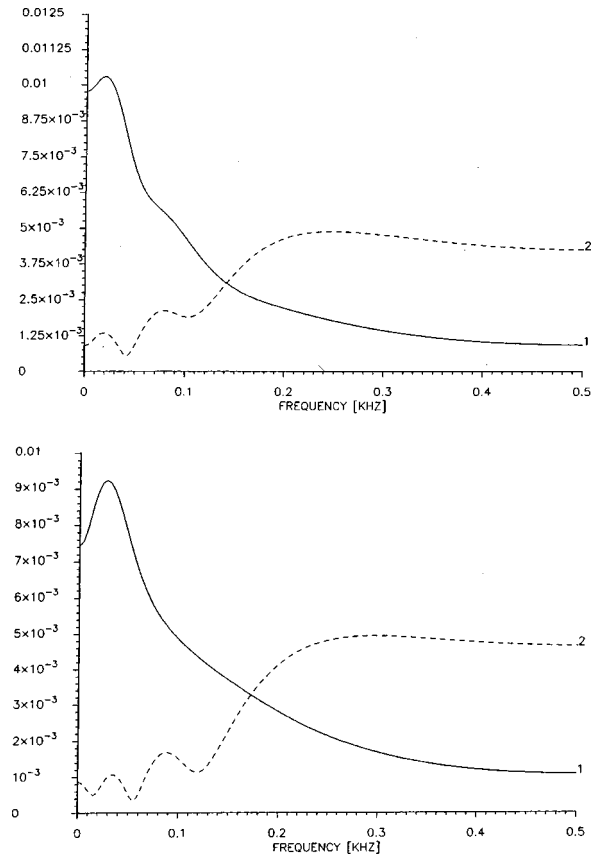

FIGURE 11. The computed two PDMs for the potential data in the frequency domain (i.e., FFT magnitude of the PDMs shown in Fig. 10). As previously, the high-pass characteristic of the second PDM is not evident in the first-order kernel (nonlinear adaptation). The two PDMs appear to divide the frequency response bandwidth, whereby the first PDM is dominant below about 150 Hz and the second PDM is dominant above that frequency.

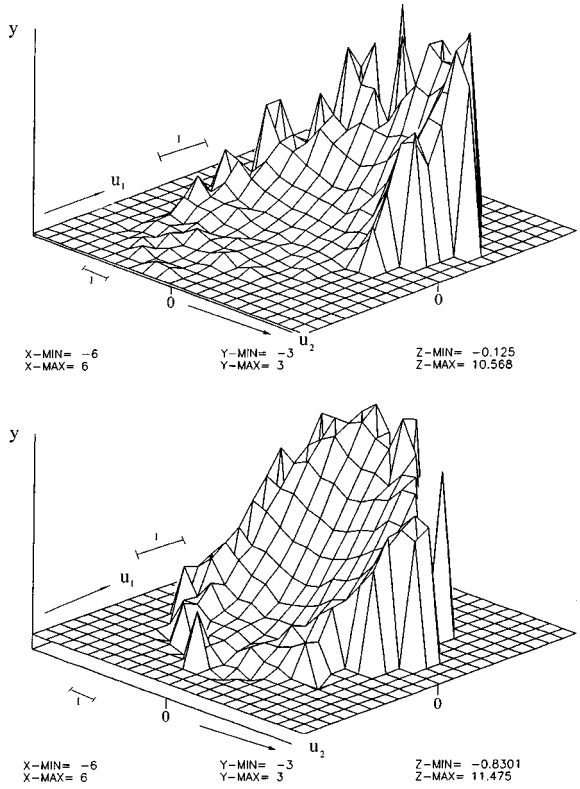

FIGURE 12. The static nonlinearities associated with the two PDMs of Figs. 10 and 11 for high (bottom) and low (top) mean displacement levels. The axes (u_1, u_2) represent the two PDM outputs, and the vertical axis is the intracellular potential response. The axes ranges are given at the bottom of each plot. The convex nonlinear characteristic is evident, as well as the even symmetry with respect to u_2. The ordinate axis units are: mV. The u_1 and u_2 axes are also in mV units (1 mV bar shown).

(11) For the intracellular current data, the concave nonlinearity exhibits threshold characteristics with respect to the output of the first mode (u_1); with the threshold being regulated by the output of the second mode (u_2). Specifically, for $u_2 \geq 0$, the threshold with respect to u_1 is almost constant at approximately $u_1 = 0$ and the slope of the suprathreshold response is large; however, for $u_2 < 0$, this threshold gradually decreases while the slope of the suprathreshold response also decreases. This nonlinear characteristic reflects the asymmetrical response of the mechanoreceptor.

(12) For the intracellular potential data, the convex nonlinearity exhibits low values for $u_1 < 0$ and rising values for $u_1 > 0$. The dependence on u_2 is even symmetric (i.e., irrespective of its sign), exhibiting higher response values for larger $|u_2|$. Since the sign of u_2 (direction of displacement change) does not seem to affect the response, the intracellular potential response is not velocity sensitive but speed sensitive.

DISCUSSION

The presented results show that the nonlinear dynamic behavior of the slit-sense organ neurons can be described by a compact model consisting of two PDMs and a two dimensional static nonlinear function. The models for the receptor current and receptor potential differ primarily in the change of the low-pass characteristics of the first PDM, reflecting the low-pass filtering of the receptor current by the membrane capacitance and resistance, as previously observed.[6] The second PDM is similar in waveform for current and potential data, endowing the mechanoreceptor with its high-pass response characteristics (akin to differentiation) that give it adaptation capabilities. These high-pass characteristics were shown to reside entirely in the second-order kernel (nonlinear adaptation). The similarity of the second PDMs for the receptor current and receptor potential supports the idea that the receptor potential is primarily a low-pass filtered version of the receptor current. This is to be expected if there are not very large changes in membrane potential

during the current clamp recordings, since the current through the mechanoreceptor channels is carried almost entirely by sodium ions[3] whose equilibrium potential is large and positive compared to the resting membrane potential.

The form of the nonlinearity in the current data resembles threshold behavior akin to half-wave rectification (with a negative slope) for positive values of the second mode ($u_2>0$), i.e., an increase of stimulus displacement values elicits strong negative current for positive displacement values but not for negative displacement values. For $u_2<0$, the aforementioned u_1 threshold is reduced for increasing $|u_2|$ and the slope of the suprathreshold response is also reduced (i.e., it becomes less negative). This response behavior is both position sensitive and velocity sensitive.

For the potential data, the nonlinearity exhibits initially supralinear (i.e., changing faster than linear) response characteristics for $u_1>0$ (with a positive slope) and somewhat flattened response for $u_1<0$. The effect of u_2 is even symmetric and causes increased response potential for larger $|u_2|$, also in supralinear fashion. Thus, this response behavior is position sensitive and speed sensitive (not rate directional). Note that these experiments were made under clamped conditions which may account for some of the differences in the nonlinear behavior evident in the current and potential response data. Finally, we should note that although the form of the nonlinearity for $u_1>0$ appears initially to be supralinear, it gradually becomes linear and then sublinear as u_1 increases and reaches the end of the dynamic range (i.e., sigmoidal overall shape).

The presented PDM model is more compact than its Volterra counterpart (e.g., for second-order models the numbers of free parameters are 108 and 1378, respectively); however the Volterra model includes the dynamics represented by the less significant eigenvalues/eigenvectors that are omitted from the PDM model. In this application, the improvement in prediction mean-square error was marginal and not consistent, lending support to the notion of a ''minimal model'' based on PDM analysis. Furthermore, as indicated above, the PDM model can be extended to nonlinear orders higher than second (even though limited to the selected PDMs in terms of dynamics) while the Volterra models cannot be practically extended into higher order nonlinearities because of the computational burden associated with the rapid increase in the number of free parameters. The adequacy of each model has to be judged in each particular application with regard to the objectives and the prevailing practical limitations.

The nonlinear dynamic behavior observed here agrees well with experiments using step displacements[5] where positive steps (indenting the slits) caused significant inward currents, while negative steps caused much smaller reductions in mean inward current. This nonlinear behavior was more pronounced in the initial dynamic responses to steps than in the late responses near the end of steps, as reflected in the model obtained by the high-pass properties of the second PDM that is primarily responsible for the nonlinear adaptive behavior.

The physiological system responsible for the receptor current consists of the slit cuticle between the stimulator and the dendritic sheath surrounding the neuron tip, a small, presumably fluid filled, region between the dendritic sheath and the neuronal membrane, and the mechanically activated ion channels in the neuronal membrane.[1] The important questions in interpreting the obtained nonlinear dynamic model are: (1) what physical mechanisms could correspond to the two PDMs, and (2) what is the basis of the nonlinearity? Presently, neither question can be answered with certainty. One obvious possibility for the two distinct PDMs would be the existence of two types of mechanically activated ion channels in the neuronal membrane, one type with low-pass characteristics, and the other with high-pass characteristics. However, no experimental evidence exists to support this possibility at present. Experiments that eliminate mechanotransduction by removing the permeant ions, or application of blocking chemicals, cause a gradual reduction in the amplitude of the entire response, rather than eliminating one dynamic component selectively.[3]

It seems difficult to explain the form of the nonlinearity or the response characteristics of the two PDMs by any of the known physical components between the stimulator and the neuronal membrane. While the fluid between the dendritic sheath and the neuronal membrane could conceivably cause high-pass behavior by dashpot action, it is impossible to say if this would be linear or nonlinear without more detailed knowledge of the molecular mechanics of the fluid. It seems equally likely that the nonlinear dynamics measured here reflect the properties of the mechanically activated channels or their connection to deformation of the neuronal membrane. Very little is known about the molecular structures of mechanically activated channels, or their linkages to the membrane or cytoskeleton. However, models of mechanically activated channels, based on single channel patch clamp recordings are starting to emerge.[11] The quantitative nonlinear dynamic descriptions of mechanotransduction provided here should be useful in constraining the selection process for such models in the future.

ACKNOWLEDGMENTS

This work was supported by NIH Grant No. RR-01861 (Biomedical Simulations Resource of the University of Southern California) and by the Medical Research Council of Canada.

APPENDIX

In discrete time, the general input–output relation of a stable (finite-memory) nonlinear time-invariant dynamic system is given by the discrete-time Volterra series:

$$y(n)=k_0+\sum_m k_1(m)x(n-m)+\sum_{m_1}\sum_{m_2} k_2(m_1,m_2) \times x(n-m_1)x(n-m_2)+\cdots, \quad \text{(A1)}$$

where $x(n)$ is the input and $y(n)$ is the output of the system. The ith term of the series is an i-tuple convolution of the ith-order kernel k_i with i versions of x. The Volterra kernels $(k_0,k_1,k_2,\dots)$ describe the dynamics of the system at each order of nonlinearity and constitute a complete and canonical representation of the system nonlinear dynamics.[13]

Expansion of the Volterra kernels on a complete basis $\{b_j(m)\}$ transforms Eq. (A1) into the multinomial expression:

$$y(n)=c_0+\sum_j c_1(j)\,v_j(n) +\sum_{j_1}\sum_{j_2} c_2(j_1,j_2)\,v_{j_1}(n)v_{j_2}(n)+\cdots =f(v_1,v_2,\dots,v_j,\dots), \quad \text{(A2)}$$

where

$$v_j(n)=\sum_m b_j(m)x(n-m) \quad \text{(A3)}$$

and $c_1(j)$, $c_2(j_1,j_2),\dots$ represent the expansion coefficients of the respective kernels.

The unknown expansion coefficients can be estimated in practice by linear regression of the output data $y(n)$ on the terms of the multinomial expression of Eq. (A2), as long as the expression is finite and its terms do not lead to ill conditioning of the regression matrix inversion. The latter condition can be secured when the input is sufficiently broadband. Note that for a white noise input and an orthogonal basis, the signals $\{v_j(n)\}$ have zero covariance. This fact was used by Wiener in his original suggestion for kernel estimation using covariance computations.[15] He also suggested the use of Laguerre functions as an appropriate orthonormal basis, owing to their built-in exponential term that makes them suitable for physical systems with asymptotically exponential relaxation dynamics.[15] This suggestion was adapted to discrete time for improved kernel estimation.[8,10,14]

The use of the kernel expansion basis implies that a general model of the Volterra class of systems can take a block-structured form wherein the basis functions $\{b_j(m)\}$ constitute the impulse responses of a filter bank whose outputs are feeding into a multi-input static nonlinearity $f(v_1,\dots,v_j,\dots)$. For a selected basis (e.g., Laguerre functions), the modeling problem reduces to estimating the multivariate function $f(\cdot)$. Of course, the latter will be different for different bases.

The PDM approach rests on the fact that, among all possible choices of expansion bases (orthogonal or nonorthogonal) there are some that require the minimum number of basis functions to achieve a given mean-square approximation of the system output. Such a minimum set of basis functions is termed the PDMs of the nonlinear system and correspond to an associated multivariate nonlinear function $f(\cdot)$ generating the system output.[9] No claim of uniqueness can be made for these PDMs or the associated nonlinearity, although the latter is unique for a selected set of PDMs for a given system and vice versa.

For the estimation of the PDMs and the output nonlinearity $f(\cdot)$ from stimulus-response data, we use eigendecomposition of a properly constructed matrix containing the estimated first and second-order kernel values (in addition to k_0), since in most practical applications kernel estimation is limited to second order. The obtained kernel values up to a maximum lag M (kernel memory) are combined to form a real symmetric $(M+2)\times(M+2)$ square matrix:

$$Q=\begin{bmatrix} k_0 & \frac{1}{2}k_1(0) & \frac{1}{2}k_1(1) & \cdots & \frac{1}{2}k_1(M) \\ \frac{1}{2}k_1(0) & k_2(0,0) & k_2(0,1) & \cdots & k_2(0,M) \\ \frac{1}{2}k_1(1) & k_2(1,0) & k_2(1,1) & \cdots & k_2(1,M) \\ \cdots & \cdots & \cdots & \cdots & \cdots \\ \frac{1}{2}k_1(M) & k_2(M,0) & k_2(M,1) & \cdots & k_2(M,M) \end{bmatrix}, \quad \text{(A4)}$$

that can be used to express the second-order Volterra model response, $y_2(n)$ in a quadratic form:

$$y_2(n)=\mathbf{x}^T(n)\,Q\mathbf{x}(n), \quad \text{(A5)}$$

where the $(M+2)$-dimensional vector $\mathbf{x}^T(n)=[1\;x(n)\;x(n-1)\cdots x(n-M)]$ is composed of the stimulus $(M+1)$-point epoch at each time n and a constant 1 that allows incorporation of the zeroth- and first-order kernel contributions in Eq. (A5). Since Q is a real symmetric square matrix, there always exists an orthonormal matrix R such that $Q=R^T\Lambda R$, leading to the expression

$$y_2(n) = \mathbf{u}^T(n) \Lambda \mathbf{u}(n), \tag{A6}$$

where Λ is the diagonal eigenvalue matrix and

$$\mathbf{u}(n) = R\,\mathbf{x}(n) \tag{A7}$$

is the vector of transformed inputs by the orthonormal eigenvector matrix R. Inspection of the real eigenvalues in Λ allows selection of the significant ones on the basis of relative magnitude (a selection that calls for appropriate threshold criteria) and subsequent selection of the corresponding orthonormal eigenvectors that become the PDMs of this system.

For each significant eigenvalue λ_i, the values of the corresponding eigenvector, $\mu_i^T = [\mu_{i,0}\, \mu_{i,1} \cdots \mu_{i,M+1}]$ (with the exception of $\mu_{i,0}$), define the ith PDM:

$$p_i(m) = \sum_{j=1}^{M+1} \mu_{i,j}\, \delta(m-j+1), \tag{A8}$$

where $\delta(\cdot)$ denotes the discrete impulse function (Kronecker delta). The obtained ith PDM generates the ith mode output $u_i(n)$ via convolution with the stimulus $x(n)$. Note that a constant offset value $\beta_i = \mu_{i,o}$ must be added to the ith mode output u_i to express the second-order model prediction $\hat{y}_2$ using J PDMs:

$$\hat{y}_2(n) = \sum_{i=1}^{J} \lambda_i [u_i(n) + \beta_i]^2. \tag{A9}$$

Nonzero offset values $\{\beta_i\}$ give rise to linear terms in $\{u_i\}$ in the model output equation.

Equation (A9) indicates that the relative importance of $u_i(n)$ for the second-order model response $\hat{y}_2(n)$ is determined by the relative magnitude (absolute value) of the corresponding eigenvalue λ_i. Note that the matrix Q is not positive definite and, therefore, negative and positive eigenvalues are possible.

In practice, the selection of the significant eigenvalues/eigenvectors must take into account signal-to-noise ratio (SNR) considerations (i.e., setting the selection threshold higher for lower SNR) and tradeoffs between prediction accuracy and model compactness. A simple selection criterion is used in this study, whereby the selected eigenvalues account for at least 90% of the output signal power.

Clearly, when the actual system is of higher than second order, the search for PDMs based on the quadratic form of Eq. (A5) may be unduly confined. Nonetheless, the final model (which includes the estimated multi-input static nonlinearity) is not limited to the second order of the employed quadratic form, since the multivariate nonlinear function of the model (receiving as inputs the outputs of the J selected PDM filters) can be estimated up to any degree of nonlinearity. There is no guarantee that the PDMs selected from the quadratic model will be adequate for the high-order model; their adequacy will be assessed ultimately by the predictive ability of the resulting model. Thus, for every time instant n, we have

$$y = F(u_1, \ldots, u_J) + \varepsilon, \tag{A10}$$

where ϵ is an error term and $F(\cdot)$ represents the nonlinear function of the model with the selected PDMs in the filter bank [i.e., in general an approximation of the associated system nonlinearity $f(\cdot)$]. The error term ϵ includes noise effects, measurement errors, and modeling errors due to the omission of less significant terms associated with small eigenvalues or the omission of PDMs residing in kernels of order higher than second. Estimates of $F(\cdot)$ can be obtained from the data, either analytically or graphically.

Analytical evaluation of $F(\cdot)$ requires the introduction of a postulated mathematical structure (form) for F, containing certain unknown parameters which are subsequently estimated from the data via least-squares fitting.

Graphical evaluation of $F(\cdot)$ is feasible when there are only two PDMs generating the outputs (u_1, u_2) then a surface can be computed in (u_1, u_2, y) space by averaging all the data y that correspond to each specified two-dimensional bin in the (u_1, u_2) plane. The graphical approach is used in this paper.

REFERENCES

[1] Barth, F. G. De sensorische apparat der spaltsinnesorgane (*Cupiennius Salei* keys, Aranae). *Z. Sellforsch* 112:212–246, 1971.

[2] French, A. S., and V. Z. Marmarelis. Nonlinear neuronal mode analysis of action potential encoding in the cockroach tactile spin neuron. *Biol. Cybern.* 73:425–430, 1995.

[3] Höger, U., P. H. Torkkeli, E. A. Seyfarth, and A. S. French. Ionic selectivity of mechanically activated channels in spider mechanoreceptor neurons. *J. Neurophysiol.* 78:2079–2085, 1997.

[4] Juusola, M., A. E. Seyfarth, and A. S. French. The sodium-dependent receptor current in a new mechanoreceptor preparation. *J. Neurophysiol.* 72:3026–3028, 1994.

[5] Juusola, M., and A. S. French. Transduction and adaptation in spider slit sense organ mechanoreceptors. *J. Neurophysiol.* 74:2513–2523, 1995.

[6] Juusola, M., and A. S. French. The efficiency of sensory information coding by mechanoreceptor neurons. *Neuron* 18:959–968, 1997.

[7] Marmarelis, V. Z. Coherence and apparent transfer function measurements for nonlinear physiological systems. *Ann. Biomed. Eng.* 16:143–157, 1988.

[8] Marmarelis, V. Z. Identification of nonlinear biological sys-

tems using Laguerre expansions of kernels. *Ann. Biomed. Eng.* 21:573–589, 1993.
[9] Marmarelis, V. Z. Modeling methodology for nonlinear physiological system. *Ann. Biomed. Eng.* 25:239–251, 1997.
[10] Ogura, H. Estimation of Wiener kernels of a nonlinear system and a fast algorithm using digital Laguerre filters. 15th NIBB Conference, Okazaki, Japan, 1985, pp. 14–62.
[11] Sachs, F. Stretch-sensitive ion channels: An update. *Sens. Transduction* 15:241–260, 1992.
[12] Seyfarth, E. A., and A. S. French. Intracellular characterization of identified sensory cells in a new mechanoreceptor preparation. *J. Neurophysiol.* 71:1422–1427, 1994.
[13] Volterra, A. Theory of Functions and of Integral and Integro-Differential Equations. New York: Dover, 1930.
[14] Watanabe, A., and L. Stark. Kernel method for nonlinear analysis: Identification of a biological control system. *Math. Biosci.* 27:99–108, 1975.
[15] Wiener, N. Nonlinear Problems in Random Theory. New York: The Technology Press of MIT and Wiley, 1958.